Burns & Trauma, 2021, 9, tkab014
https://doi.org/10.1093/burnst/tkab014
Technical Report

Technical Report

A novel method for objectively, rapidly and accurately evaluating burn depth via near infrared spectroscopy

Meifang Yin[1], Yongming Li[2], Yongquan Luo[3], Mingzhou Yuan[4], Ubaldo Armato[1,5], Ilaria Dal Prà[5], Lijun Zhang[1], Dayong Zhang[3], Yating Wei[1], Guang Yang[1], Lixian Huang[3], Pin Wang[2,*] and Jun Wu[1,*]

[1]Department of Burn and Plastic Surgery, Institute Translational Medicine, The First Affiliated Hospital of Shenzhen University, Shenzhen Second People's Hospital, Shenzhen 518035, China, [2]School of Microelectronics and Communication Engineering, Chongqing University, Chongqing 400044, China, [3]Institute of Fluid Physics, China Academy of Engineering Physics, Mianyang, Sichuan 621900, China, [4]Department of Burn Surgery, The First Affiliated Hospital, Sun Yat-sen University, Guangzhou 510080, China and [5]Human Histology & Embryology Section, Department of Surgery, Dentistry, Pediatrics & Gynecology, University of Verona Medical School, Strada Le Grazie 8, Verona 37134, Italy

*Correspondence. Pin Wang, Email: wangpin@cqu.edu.cn; Jun Wu, Email: junwupro@126.com

Received 7 September 2020; Revised 27 December 2020; Editorial decision 30 March 2021

Abstract

The accurate and objective evaluation of burn depth is a significant challenge in burn wound care. Herein, we used near infrared spectroscopy (NIRS) technology to measure the different depth of thermal burns in *ex vivo* porcine models. Based on the intensity of the spectral signals and the diffuse reflection theory, we extracted the optical parameters involved in functional (total hemoglobin and water content) and structural (tissue scattered size and scattered particles) features that reflect the changes in burn depth. Next, we applied support vector regression to construct a model including the optical property parameters and the burn depth. Finally, we histologically verified the burn depth data collected via NIRS. The results showed that our inversion model could achieve an average relative error of about 7.63%, while the NIRS technology diagnostic accuracy was in the range of 50 μm. For the first time, this novel technique provides physicians with real-time burn depth information objectively and accurately.

Key words: Burn depth, Near infrared spectroscopy, Support vector regression

Highlights

- This study is the first to use near infrared technology to determine the depth of burn tissue.
- This study is the first to apply support vector regression to construct a model that includes the optical property parameters and the depth value of burn tissue.
- This study is the first to realize nanometer accuracy of burn depth diagnosis.

Background

The treatment of burns depends on the depth of skin injury and the extent of the burned area [1]. However, current diagnosis of burn depth is subjective, i.e. using the naked eye, the accuracy of which depends on a physician's skill. In practice, it is relatively easy to recognize very superficial or full thickness burn injuries. Conversely, distinguishing superficial from deep partial thickness burns remains the most difficult endeavor of burn wound depth assessment [2, 3]. Previous reports proved that the most skilled burn surgeons could assess burns depth with about 70% accuracy [4].

Various diagnostic tools, such as laser Doppler imaging (LDI) [5], optical coherence tomography [6], near infrared spectroscopy (NIRS) [7], terahertz imaging [8], spatial frequency domain imaging [9] and indocyanine green (ICG) fluorescence [2], have been used to evaluate burn depth [10]. At present, commercial LDI systems have become a mature technology and can be used for the clinical diagnosis of burn depth, especially for superficial and deep partial thickness burn wounds [11]. The LDI signal is based on changes in local tissue blood flow; however, the acceptable accuracy of burn degree diagnosis is limited to a maximum of 48 hours after the injury [12]. Reportedly, ICG fluorescence technology showed a certain accuracy in a limited number of human experiments [2] but interpretation of the fluorescent image is subjective. At the same time, the ICG technique requires intravenous injection of a fluorescent dye, which limits its clinical application. Many studies have shown that NIRS allows diagnosis of burns of different degrees based on the amount of oxy-hemoglobin, de-oxyhemoglobin, water content and total hemoglobin, which are all important parameters of burn injuries [7, 13–15]. However, these studies only aimed to improve the accuracy of assessment of the degree of burn injuries (superficial, partial thickness and full thickness burns) to determine whether to carry out surgery. The purpose of this study was to use NIRS to evaluate burn depth and compare this with the gold standard of pathological detection, so as to provide the basis for accurate debridement in the future.

Methods

Study design

All animal studies were approved by the Management Committee of Laboratory Animals Use of the Shenzhen Translational Medicine Institute (AUP-190708-YMF-002). A total of 5 Bama miniature pigs, each aged 4 months, were used in this study.

Collagen fiber models and analyses

The collagen I (Sigma, USA) solution was diluted to a concentration of 250 μg/dL with phosphate buffered saline. The thermo-denaturation group was incubated in a 100°C water bath for 1 minute, after which the samples were loaded into the sample console for Atomic Force Microscope detection.

Animals and anesthesia

The pigs were sedated with 25 mg/kg sodium pentobarbital (concentration, 2%) (Shanghai Chemical Reagent Company, China) via marginal ear vein injection. The flank and back hairs were trimmed with electric clippers and the skin was scrubbed with soap and water. While still sedated, the pigs were killed by an intracardiac injection of pentobarbital and dissected away the skin.

NIR diffuse reflectance spectroscopy measurements

The NIRS system consists of a spectrometer (NIR-Quest 256–2.1, Ocean Optics, USA), a tungsten halogen lamp (HL 2000, Ocean Optics, USA) and a fiberoptic probe (QP600–2, Ocean Optics, USA). The spectral range varies from 900–2200 nm and the spectral resolution is 4.91 nm when co-adding 64 scans.

Burn models and analyses

Contact thermal burns were created on the *ex vivo* pig skin using a round metal hot iron (diameter, 2 cm) of a temperature-controlled burner (Ltd YLS-5Q, Beijing Zhongshi Di Chuang Technology Development Co., China). The temperature of the metal head was set at 100°C. The hot iron was applied to the *ex vivo* pig skin for 5, 10, 20, 30, 40 and 60 seconds in order to create burns of different depths. After collecting the spectral data, the skin tissue was harvested, fixed in 10% formalin and the specimens were stained with Masson trichrome. Each burn depth was measured 5 times by 2 independent researchers. Next, the average histological depth served as the golden standard of the burn depth.

Data analysis

After smoothing all the data and removing the outliers, the experimental data were obtained. The total number of data samples was 1557. The diffuse theory [16] was used to analyse the contents of the extracted component information (Hb, HbO_2 and H_2O) and the structural information (A, β) to characterize the functional status of the burned skin. The above parameters represent the optical properties of the burned skin. The expression of diffuse reflection is as follows:

$$R(\lambda) = A\left(\frac{\lambda}{\lambda_0}\right)^{-\beta} \cdot e^{-\left(a_{Hb}\cdot A_{Hb}(\lambda)+a_{HbO_2}\cdot A_{HbO_2}(\lambda)+a_{H_2O}\cdot A_{H_2O}(\lambda)\right)}$$

where A is proportional to the density of the scattering particles and is related to the average scatter size. $A_{HbO_2}(\lambda)$is the absorption coefficient of oxygenated hemoglobin and $A_{Hb}(\lambda)$is the absorption coefficient of deoxygenated hemoglobin [17]. $\alpha_{HbO_2}$and α_{Hb} are the contents of oxygenated hemoglobin and deoxygenated hemoglobin, respectively. The total hemoglobin is equal to α_{HbO_2}

plus α_{Hb}. The A_{H_2O} and α_{H_2O} are the water absorption coefficient [18] and water content, respectively. The selected central wavelength of the wave band is λ_0. By calculating and minimizing the error between $R(\lambda)$ and original measured diffuse spectral data , we obtain the parameters.

We employed the obtained characteristic parameter samples for support vector regression (SVR) training. We used SVR to develop the burn depth inversion model according to the information provided by the 4 parameters. The output value of the radial basis kernel function of the inversion model was the estimated value of burn depth.

The training set and test set were divided into 2 groups using the hold-out method. Two-thirds of the samples (1037 samples) were randomly selected as training samples, and one-third of the specimens (520 samples) were used as test samples. We used the inversion model to classify and identify each test sample. We performed every classification experiment 10 times and then calculated the precision of the inversion model.

Results

Changes of collagen fibers after thermal injury

The predominant extracellular matrix component of the skin is collagen. The structural alteration of collagen may correspond to the damage level of burned skin and be detectable by NIRS imaging. Therefore, we used atomic force microscopy to observe the possible structural changes of overheated collagen fibers. After thermo-denaturation, the helical structure of the collagen fibers completely disappeared, instead being transformed into sand-like particles (Figure 1). The 3D synthesis diagram showed the profound alteration of the structure of the collagen, with total loss of orientation and severe fragmentation of the fibers (Figure 2).

Establishing thermal injury models with different burn depths

We created a total of 6 different burn depth models by changing the hot iron contact time [9]. As shown in Figure 3, by lengthening the contact time the color of the skin in the damaged areas became darker while the boundary with normal skin became sharper. Masson staining showed the neat boundary between necrotic and normal tissues (Figure 4), and in these pig models the depth of the thermal injuries ranged from 92 μm to 1010 μm, spanning superficial to full thickness burns (Table 1).

Analysis of structural and functional parameters correlated with histological burn depth

Figure 5 shows that the reflectance spectra obtained with NIRS pertaining to 6 different burn depths overlapped at the

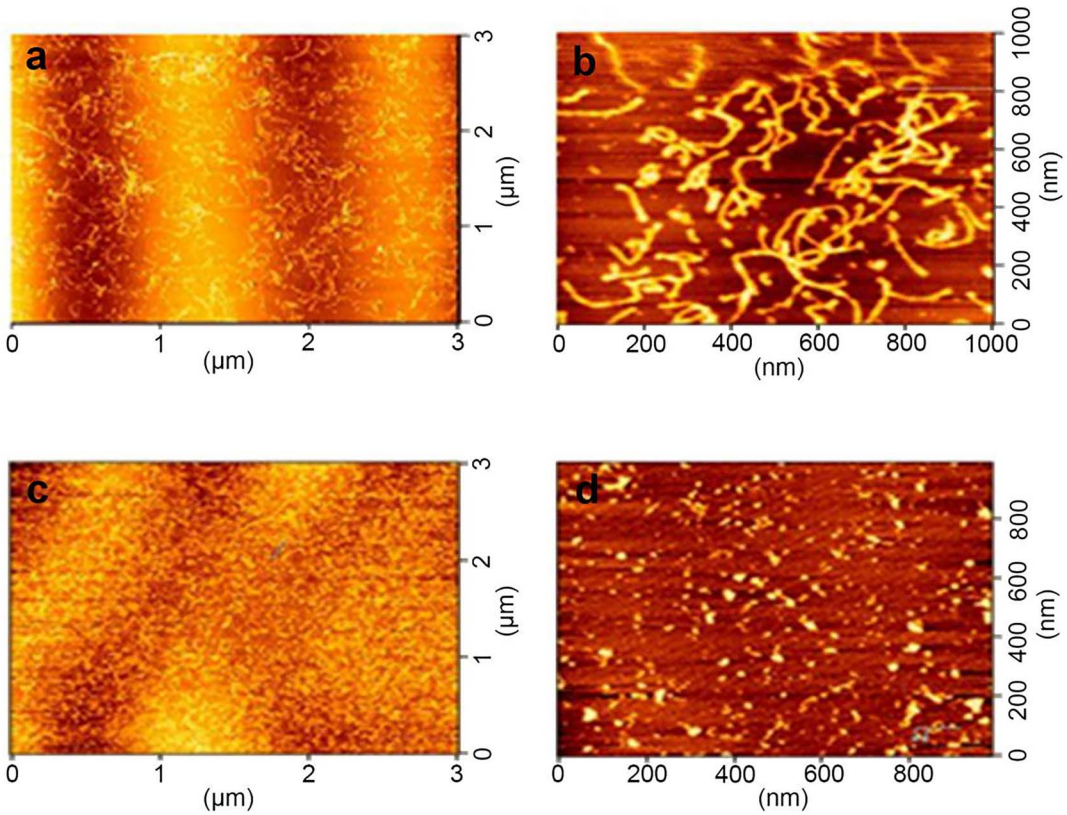

Figure 1. Atomic force microscopy reveals the deep structural changes of collagen fibers after a thermal injury: (**a**) normal collagen fibers, (**b**) high magnification view of normal collagen fibers, (**c**) burned collagen fibers, and (**d**) high magnification view of burned collagen fibers

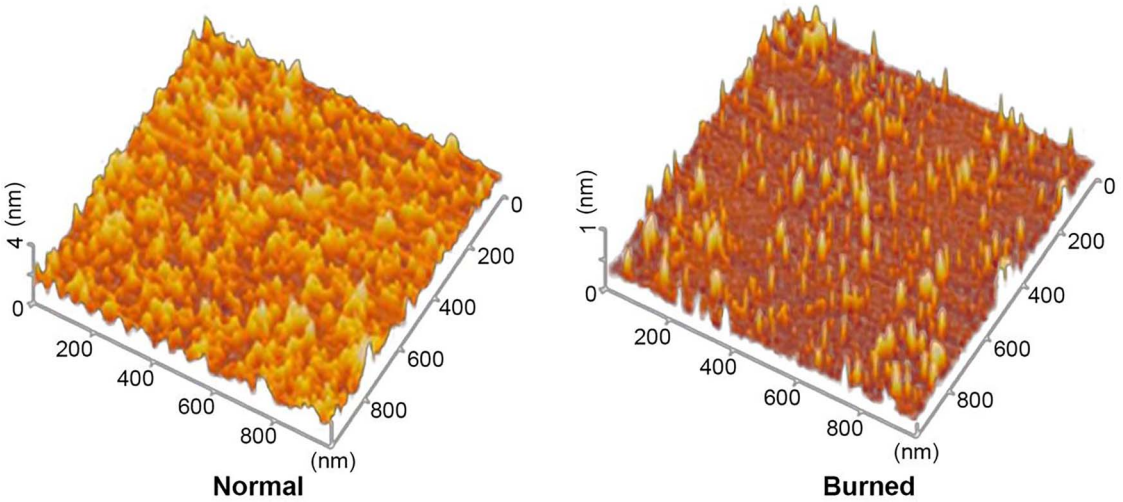

Figure 2. Three-dimensional synthesis of the collagen fibers spatial distribution under healthy and burned conditions

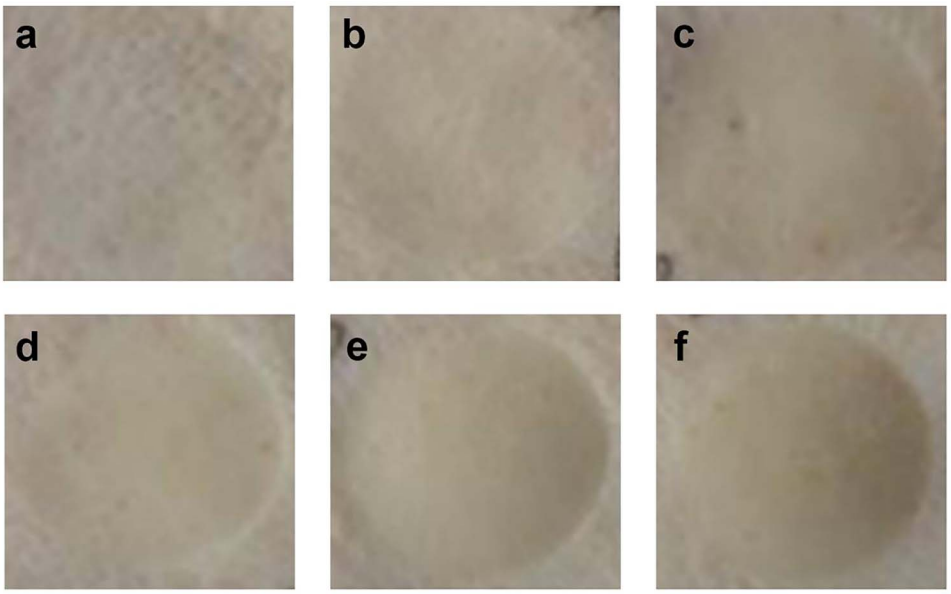

Figure 3. Thermal injury models of different depths. The contact time between the hot iron and the pig skin surface: (**a**) 5s, (**b**) 10s, (**c**) 20s, (**d**) 30s, (**e**) 40s, (**f**) 60s

1150–1850 nm region. To characterize the burned skin, we used Monte Carlo analysis to extract both the functional (i.e. total hemoglobin and water content) and structural (i.e. scattering size β and density of scattering particles A) information parameters as the features typical of burn depth. Scattering size and scattering particles were suitable for describing the structural condition of the tissue, such as collagen fibril diameter and density, since the size and distribution of collagen fibers were the main sources of skin scattering signals [18].

Figure 6 shows the relationship between the functional and structural information parameters and the different degrees of burns. As burn depth increased the water content tended to decrease. In turn, the decrease in water content slowly increased the total hemoglobin concentration and collagen fibril density. Thus, we found that the scattering intensity tended to decrease, which was consistent with the changes in the spatial structure and diameter of collagen fibrils elicited by the burn (Figures 1–2). These results proved that the method could extract the information about the structure and function of the burned skin.

Burn depth evaluation based on the SVR model

We selected the above mentioned 4 parameters (total hemoglobin parameters, water content parameters, scattering particles size β parameters, density of scattering particles A) as the initial features to predict burn depth, as the burn depth was obviously related to them. Thus, we used SVR to develop the burn depth inversion model according to the information provided by the 4 parameters. To this end, we randomly selected two-thirds of the samples as training specimens. We used the remaining one-third of the samples

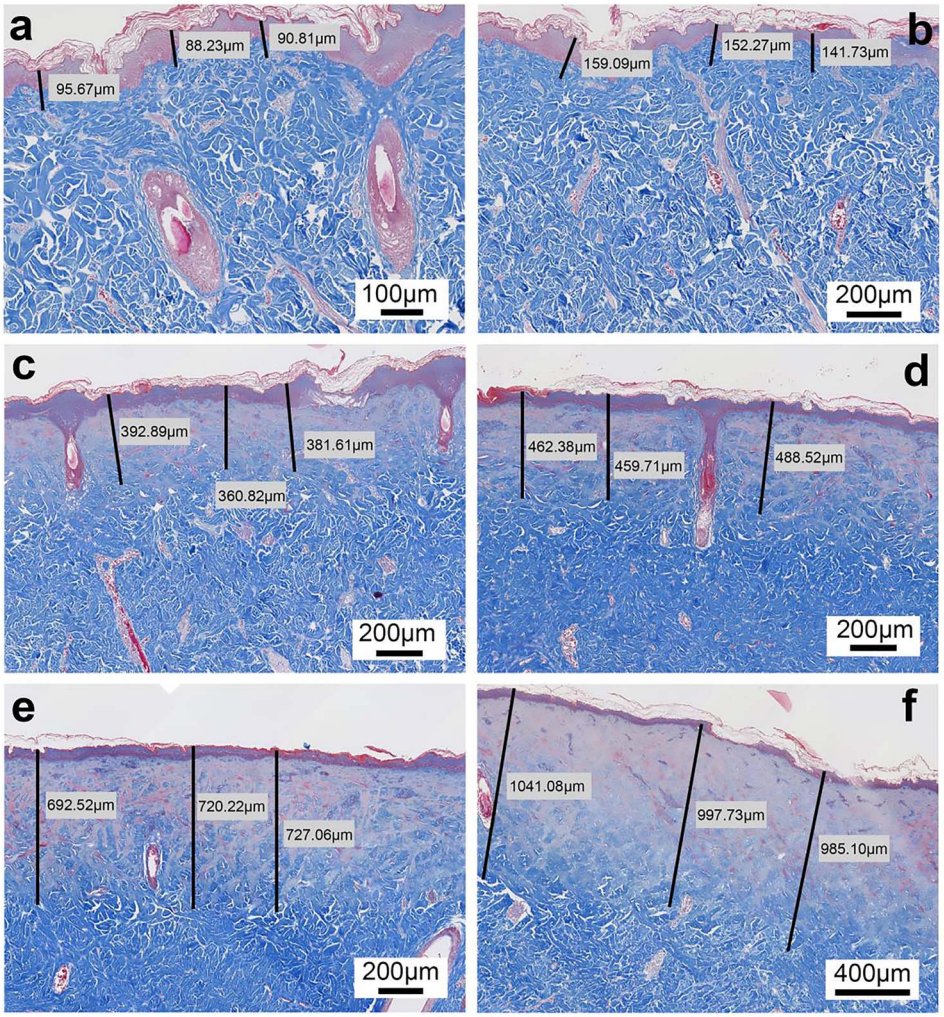

Figure 4. Masson trichrome-stained slides of thermally injury tissues. The contact time between the hot head and the pig skin surface: (**a**) 5s, (**b**) 10s, (**c**) 20s, (**d**) 30s, (**e**) 40s, (**f**) 60s. The black bars represent the depth of thermal injury

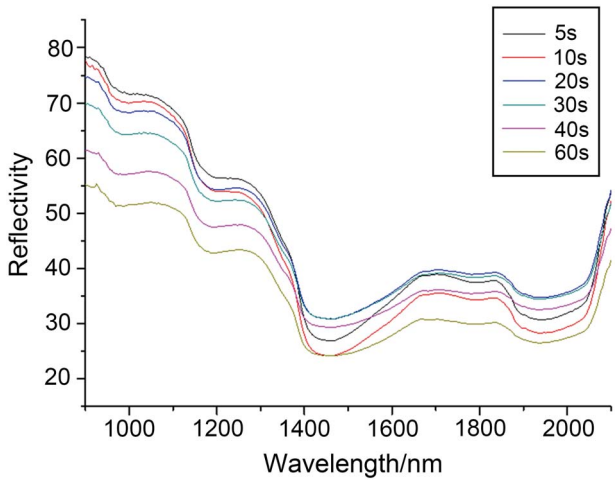

Figure 5. Original near infrared spectroscopy curves of different times of hot head application

to test the inversion model of burn depth. Table 1 shows the results of the average predicted burn depths based on SVR. The experiment was repeated 10 times under the same conditions. By comparing the predicted burn depth with the histological burn depth, we found that the average relative error was 7.63% (Table 1). The predicted burn depth was close to the histological burn depth. Table 1 shows the results of the average predicted burn depths based on SVR.

Discussion

It is worth recalling that NIRS has many advantages over other detection methods. First, near infrared photons penetrate more deeply (up to 5–10 mm) into living tissues [20]. Second, it is a non-invasive, low-cost device that does not need any chemical reagent, such as ICG dye [21]. Third, unlike orthogonal polarization spectroscopy, which requires direct contact with the wound, NIRS diagnosis avoids cross infection [22]. Last, when compared to traditional high-frequency ultrasonic and pathological methods, NIRS results do not depend upon subjective appraisals and can be gained in only 1 minute [23]. Altogether these advantages indicate that NIRS technology can be used as an ideal objective technique to diagnose burn depth.

Table 1. Pathological burn depth values, average predicted burn depth values and inversion model predicting the average relative error of 10 tests for each different hot iron application time

Time	5 s	10 s	20 s	30 s	40 s	60 s
Pathological depth (μm)	92 ± 4	151 ± 9	378 ± 16	470 ± 16	713 ± 18	1008 ± 29
Predicted depth (μm)	120 ± 12	164 ± 5	329 ± 18	462 ± 9	709 ± 7	$1008 \pm 3 \times 10^{-2}$
Relatively error (%)	30.9 ± 13.1	8.7 ± 3.2	13.1 ± 4.7	1.9 ± 1.8	0.4 ± 0.9	$(3.0 \pm 2.0) \times 10^{-3}$

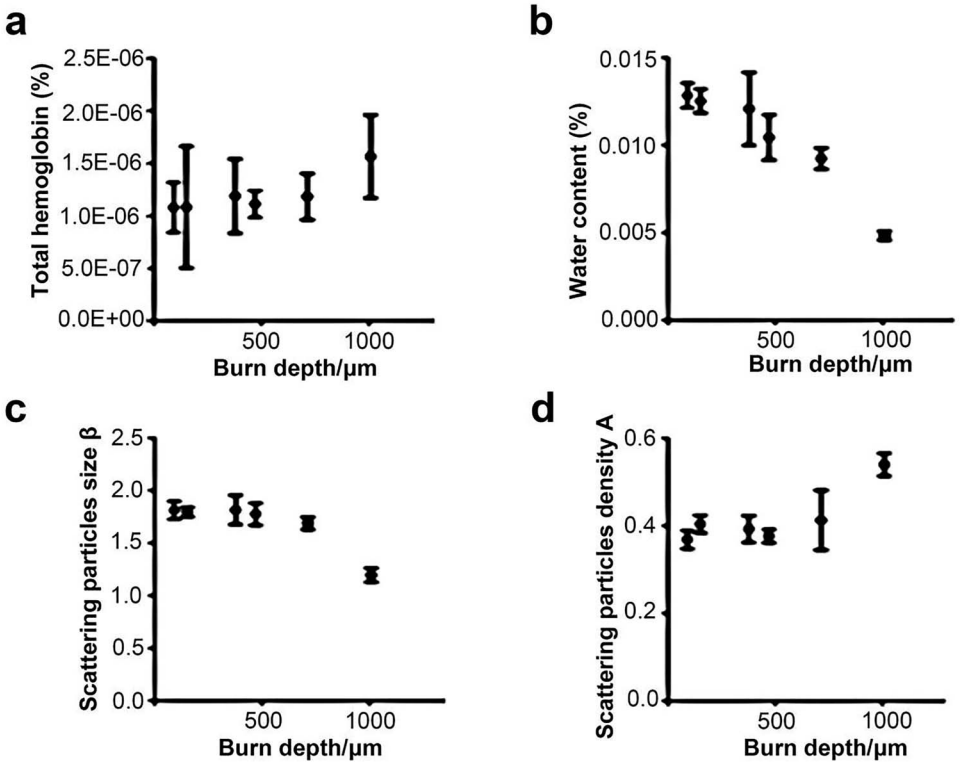

Figure 6. Relationship between extraction parameters and scald depth: (**a**) total hemoglobin parameters, (**b**) water content parameters, (**c**) scattering particles size β parameters, and (**d**) scattering particles density A parameters

As with the classical assessment of burn degree based on visual signs such as color and swelling, NIRS is a multivariate technology allowing simultaneous assessment of many of these signs. The diffuse reflectance spectrum of the skin is characterized by absorption and scattering spectra [24]. The knowledge of the data about such absorption and scattering spectra provides information about the tissue composition and its structural parameters, respectively [25, 26].

Previous studies have confirmed that NIRS can quickly and non-invasively diagnose the different degrees of burns on the basis of the amount of total hemoglobin, hemoglobin oxygen saturation, HbO_2, Hb and the water content of injured tissue [7, 13–15]. According to literature reports, partial thickness injuries are difficult to differentiate on the basis of tissue oxygenation measurements made within the first 3 hours following the injury. Intermediate and deep partial thickness burns have oxygenation levels that show small differences, whereas more severe injuries exhibit distinctly lower oxygenation levels [13]. According to previous research, we used 2 better-performing experimental parameters, total hemoglobin and water content, which can be used as indicators of tissue function (i.e. tissue composition).

In addition to changes in tissue function after a burn injury, changes in tissue structure also occur. As shown in the Masson trichrome-stained slides (Figure 4), thermal damage causes collagen denaturation and effectively melts collagen fibrils. This is the most dramatic change compared to normal skin and is consistent with the results found in the literature that the size and distribution of collagen fibrils are the primary contrast mechanism for scattering signals in the skin [19]. Therefore, we choose 2 structural parameters, scattering size and scattering particles, which are suitable for describing the diameter and density of collagen fibers. To sum up, we selected 4 optical parameters representing the composition and structure of the burned tissue to optimally establish our diagnosis model of burn depth.

The relationship between these parameters and burn depth is a non-linear regression problem with multiple inputs and

outputs. Therefore, we used the SVR inversion model to detect the depth of the burned skin. From the results of the Monte Carlo analysis, we found that the changes of the 4 parameters were truly consistent with the alterations of the structure and function occurring at different burn depths. Thus, we argued that a multivariate analysis, taking into account the total hemoglobin, water content, scattering size and scattering particles parameters, could jointly and dramatically improve the reliability and robustness of the NIRS when applied to burn depth evaluation. Our model accurately established the complex relationships intervening between NIRS signals and burn depths.

Previous studies could not satisfactorily improve the diagnostic accuracy of the degree of a burn injury and do not provide factual information about burn depth. Our results prove for the first time that it is possible to accurately and quantitatively assess the depth of burns with an average relative error amounting to less than 10% (in fact, only 7.63%). The burn depth predicted via our method was close to the histologically assessed burn depth—the error is about 50 μm. The advantages of NIRS diagnosis of burn depth, compared with other methods that only determine the degree of burn injuries, is that NIRS can provide the exact thickness of the injured tissue, so as to provide guidance around how much tissue to remove during debridement surgery in the future.

In this experiment, we used pig skin *ex vivo* to eliminate the interference of age, edema, heartbeat fluctuation and other factors on the NIRS signal. After the preliminary establishment of the detection model, we found that age, injury site and other clinical factors were a great challenge to the diagnostic accuracy of the model. As more clinical factors are added to the model, the interaction of all factors will add value to its accuracy.

Conclusions

We have presented results demonstrating that the accuracy of NIRS technology in detecting the burn depth in *ex vivo* models falls in the range of microns. The fact that NIRS can accurately detect burn depth in real time in a non-invasive and contactless way hopefully represents a great opportunity to improve burn diagnosis and treatment. Our present work has laid the foundation for further algorithm developments and clinical applications.

Abbreviations

ICG: indocyanine green; LDI: laser Doppler imaging; NIRS: near infrared spectroscopy; SVR: support vector regression

Funding

This work was supported by grants from the National Natural Science Foundation of China (No. 81701904).

Availability of data and materials

All data generated or analysed during this study are included in this published article.

Authors' contributions

JW, PW and MY conceived and designed the study. MY, MY, LZ, YW and GY performed the biological experiments. LH, YL and DZ were responsible for hardware development. PW and YL conducted data analysis. MY, JW and UA discussed and wrote the manuscript. All authors read and approved the final manuscript.

Ethics approval and consent to participate

All animal studies have been approved by the Management Committee of Laboratory Animals Use of the Shenzhen Translational Medicine Institute.

Conflicts of interest

The authors declare that there is no conflict of interest.

References

1. Islam A, Ingrid S, Mats F, Folke S, Moustafa E. Use of the burn intervention score to calculate the charges of the care of burns. *Burns*. 2019;45:303–9.
2. Dissanaike S, Abdul-Hamed S, Griswold J. Variations in burn perfusion over time as measured by portable ICG fluorescence: a case series. *Burns Trauma*. 2014;2:201–5.
3. Khatib M, Jabir S, Fitzgerald O, Connor E, Philp B. A systematic review of the evolution of laser doppler techniques in burn depth assessment. *Plast Surg Int*. 2014;2014:621792. doi: 10.1155/2014/621792.
4. Monstrey S, Hoeksema H, Verbelen J, Pirayesh A, Blondeel P. Assessment of burn depth and burn wound healing potential. *Burns*. 2008;34:761–9.
5. Wang R, Zhao J, Zhang Z, Cao C, Zhang Y, Mao Y. Diagnostic accuracy of laser doppler imaging for the assessment of burn depth: a meta-analysis and systematic review. *J Burn Care Res*. 2020;41:619–25.
6. Deegan AJ, Mandell SP, Wang RK. Optical coherence tomography correlates multiple measures of tissue damage following acute burn injury. *Quant Imag Med Surg*. 2019;9:731–41.
7. Cross KM, Leonardi L, Payette JR, Gomez M, Levasseur MA, Schattka BJ, *et al*. Clinical utilization of near-infrared spectroscopy devices for burn depth assessment. *Wound Repair Regen*. 2007;15:332–40.
8. Dutta M, Bhalla AS, Guo R. THz imaging of skin burn: seeing the unseen—an overview. *Adv Wound Care*. 2016;5:338–48.
9. Mazhar A, Saggese S, Pollins AC, Cardwell NL, Nanney L, Cuccia DJ. Noncontact imaging of burn depth and extent in a porcine model using spatial frequency domain imaging. *J Biomed Opt*. 2014;19:086019. doi: 10.1117/1.
10. Nian YJ, Chen ZQ, Xue DD, Yin MF. Advances in the research of diagnosis techniques of burn depth. *Chin J Burns*. 2016;32:698–701.
11. Jan SN, Khan FA, Bashir MM, Nasir M, Ansari HH, Shami HB, *et al*. Comparison of laser doppler imaging (LDI) and clinical

assessment in differentiating between superficial and deep partial thickness burn wounds. *Burns*. 2018;44:405–13.
12. Hoeksema H, Van de Sijpe K, Tondu T, Hamdi M, Van Landuyt K, Blondeel P, *et al*. Accuracy of early burn depth assessment by laser doppler imaging on different days post burn. *Burns*. 2009;35:36–45.
13. Sowa MG, Leonardi L, Payette JR, Fish JS, Mantsch HH. Near infrared spectroscopic assessment of hemodynamic changes in the early post-burn period. *Burns*. 2001;27: 241–9.
14. Sowa MG, Leonardi L, Payette JR, Cross KM, Gomez M, Fish JS. Classification of burn injuries using near-infrared spectroscopy. *J Biomed Opt*. 2006;11:054002. doi: 10.1117/1.2362722.
15. Cross KM, Leonardi L, Gomez M, Freisen JR, Levasseur MA, Schattka BJ, *et al*. Noninvasive measurement of edema in partial thickness burn wounds. *J Burn Care Res*. 2009;30: 807–17.
16. Zonios G, Perelman LT, Backman V, Manoharan R, Fitzmaurice M, Van Dam J, *et al*. Diffuse reflectance spectroscopy of human adenomatous colon polyps in vivo. *Appl Opt*. 1999;38: 6628–37.
17. Prahl S. *Hemoglobin absorption coefficient*. Available at: http://omlc.ogi.edu/spectra/hemoglobin/index.html. (7 Sep 2020, date last accessed).
18. Palmer KF, Williams D. Optical properties of water in the near infrared. *J Opt Soc Am*. 1974;64:1107–10.
19. Chen D, Zeng N, Xie Q, He H, Tuchin VV, Ma H. Mueller matrix polarimetry for characterizing microstructural variation of nude mouse skin during tissue optical clearing. *Biomed Opt Express*. 2017;8:3559–3570.
20. Kim NS, Jin HY, Kim EY, Hong TH. Cystic duct variation detected by near-infrared fluorescent cholangiography during laparoscopic cholecystectomy. *Ann Surg Treat Res*. 2017;92:47–50.
21. McUmber H, Dabek RJ, Bojovic B, Driscoll DN. Burn depth analysis using indocyanine green fluorescence: a review. *J Burn Care Res*. 2019;40:513–6.
22. Goertz O, Ring A, Köhlinger A, Daigeler A, Andree C, Steinau H, *et al*. Orthogonal polarization spectral imaging. *Ann Plas Surg*. 2010;64:217–21.
23. Lin Y, Huang C, Wang S. Quantitative assessments of burn degree by high-frequency ultrasonic backscattering and statistical model. *Phys Ned Biol*. 2011;56:757–73.
24. Mustari A, Kanie T, Kawauchi S, Sato S, Sato M, Kokubo Y, *et al*. In vivo evaluation of cerebral hemodynamics and tissue morphology in rats during changing fraction of inspired oxygen based on spectrocolorimetric imaging technique. *Int J Mol Sci*. 2018;19:491. doi: 10.3390/ijms19020491.
25. Zhen-huan F, Xia-ping F, Xue-ming H. Investigation of absorption and scattering characteristics of kiwifruit tissue using a single integrating sphere system. *J Zhejiang Univ Sci B*. 2016;17:484–492.
26. Taroni P, Paganoni AM, Ieva F, Pifferi A, Quarto G, Abbate F, *et al*. Non-invasive optical estimate of tissue composition to differentiate malignant from benign breast lesions: a pilot study. *Sci Rep-UK*. 2017;7:40683. doi: 10.1038/srep40683.